

# Correcting Delocalization Error in Materials with Localized Orbitals and Linear-Response Screening

Jacob Z. Williams and Weitao Yang\*

*Department of Chemistry, Duke University, Durham, NC 27708, USA*

(Dated: July 3, 2024)

Delocalization error prevents density functional theory (DFT) from reaching its full potential, causing problems like systematically underestimated band gaps and misaligned energy levels at interfaces. We introduce lrLOSC to correct delocalization error in materials over a wide range of band gaps. We predict eleven materials' fundamental gaps to within 0.28 eV, while offering a nonzero correction to the total energy. Molecular properties are improved with the same theory (arXiv:2406.06345). lrLOSC is an essential step toward modeling molecules, materials, and their interfaces within the same DFT framework.

Kohn–Sham density functional theory (DFT) [1–5] is rightly regarded as the default method for quantum-mechanical calculations in both chemistry and materials science. The availability of reasonably accurate density functional approximations (DFAs), implemented efficiently in community software, remains unparalleled decades later. Frontier orbital (or valence band maximum and conduction band minimum) energies from (generalized) Kohn–Sham DFAs have been shown to be the chemical potentials, defined as the derivatives of the associated DFA's total energy with respect to the electron number [6, 7]; the proof uses Janak's theorem [8], but extends it to functionals of the density matrix. DFA frontier orbitals thus predict the fundamental gaps of molecules and materials based on the exact conditions for fractional charges [9, 10]. But DFAs suffer systematic errors, including a characteristic and enduring underestimation of the fundamental gap [11]. Band structures obtained by (semilocal) DFAs are also quite inaccurate, and decades of work has been poured into various methods for improving them [12–17]. Accurately computing band structures, and especially band gaps, within the efficient DFT framework is a pressing problem for computational physicists, chemists and materials scientists. Predicting and aligning energy levels is critical for the development of semiconductor technology [18, 19]; solar cells [20]; and photocatalysts [21]. Interfacial band structure [22, 23] is particularly challenging because adsorbates' bands are renormalized, yet of outsize importance in predicting the properties of next-generation heterogeneous materials [24, 25]. Behind the band gap and band structure problems lies *delocalization error* [26–29].

Delocalization error in DFAs is a significantly and systematically incorrect behavior of the energy  $E$  viewed as a function of the number  $N$  of electrons as exhibited for small systems, but its manifestation depends on the size of the system [26]. The exact  $E(N)$  curve is piecewise linear, with derivative discontinuities at integer  $N$  [9, 10]; the magnitude of the discontinuity gives the fundamental gap.  $E(N)$  is convex in finite systems when calculated with typical DFAs, underestimating the derivative discontinuity and thus the gap [6]. As the size

of the system increases, however,  $E(N)$  becomes less convex. In periodic boundary conditions, piecewise linearity of  $E(N)$  is restored automatically, but deceptively: delocalization occurs across the entire infinite lattice, the derivative discontinuity is underestimated just like for finite  $N$ , and the total energy of charged bulk systems is incorrect [26]. Correcting delocalization error in both molecules and materials, then, requires that both the orbital energies and the total energy be corrected, all within the same approximation scheme.

Two ingredients—orbital localization and screening—are key to delocalization error corrections. The localized orbital scaling correction (LOSC) initially featured localization without screening [30, 31]: it was good enough to cure delocalization error in atoms' and small molecules' valence orbitals [32]. LOSC orbital energies have accuracy comparable to molecular  $GW$  [33] and can replace  $GW$  quasiparticle energies as the starting point for Bethe–Salpeter calculations of neutral excitations [34]. Screening without localization, on the other hand, is realized by the global scaling correction (especially GSC2) [35–37]. The screening in GSC2 is based on the exact second derivatives of the total energy with respect to orbital occupations [38]. GSC2 improves atomic and molecular photoemission spectra [37], as well as valence orbital energies, when orbital relaxation is included [36, 39, 40]. Although screening plays a smaller role in molecular valence ionization, both localization and screening are necessary to describe core-electron quasiparticle energies [41].

Correcting delocalization error in bulk materials also requires both localization and screening. GSC, lacking localization, offers no correction at all to the total energy of gapped materials, so it cannot restore size-consistency of the gap [30]. On the other hand, the initial version of LOSC overestimates orbital energy corrections significantly because the screening of the Coulomb repulsion by other electrons is ignored. Mahler *et al.* [42] proposed screened LOSC (sLOSC), which included an empirically screened Hartree repulsion and substantially improved the band gaps of semiconductors and insulators. But sLOSC's screening is identical for all systems, which fundamentally limits its accuracy. In this work, we ex-

tend LOSC to include the linear-response screening of GSC; we call the resulting method lrLOSC. (A parallel work [41] implements lrLOSC in molecular systems.) lrLOSC is related in spirit to Koopmans-compliant spectral functionals [43–45], the Wannier–Koopmans method [46–50], and Wannier optimally-tuned screened range-separated hybrid functionals [51, 52], all of which correct orbital energies using localized orbitals (in materials, Wannier functions) and screening of the electron-electron interaction. But unlike LOSC, these functionals do not correct the total energy of systems with integer orbital occupations—such as physical systems with a finite band gap [43]—which requires mixing of the occupied and virtual manifolds. Their corrections therefore cannot restore size-consistency to the DFA [30].

lrLOSC modifies the DFA total energy by

$$\Delta E = \frac{1}{2} \sum_{\sigma} \sum_{ij\mathbf{R}} \lambda_{\mathbf{R}ij\sigma}^* (\delta_{\mathbf{R}ij} - \lambda_{\mathbf{R}ij\sigma}) \kappa_{\mathbf{R}ij\sigma}, \quad (1)$$

where  $i, j, \sigma$  are respectively the band-like and spin indices of localized orbitals  $|w_{\mathbf{R}i\sigma}\rangle$  and  $\mathbf{R}$  indexes the primitive cell translation vectors (see below). The local occupations  $\lambda_{\mathbf{R}ij\sigma} = \langle w_{\mathbf{0}i\sigma} | \rho | w_{\mathbf{R}j\sigma} \rangle$  are elements of the density matrix  $\rho$  in the local orbital basis, and the curvature  $\kappa_{\mathbf{R}ij\sigma}$  measures the delocalization error between  $|w_{\mathbf{0}i\sigma}\rangle$  and  $|w_{\mathbf{R}j\sigma}\rangle$ .  $\delta_{\mathbf{R}ij}$  is the Kronecker delta, and  $\lambda^*$  is the complex conjugate of  $\lambda$ . Note that lrLOSC assumes a spin-polarized, collinear DFA calculation, with orthogonal Bloch spin orbitals:  $\langle \psi_{\mathbf{k}m\sigma} | \psi_{\mathbf{q}n\tau} \rangle \propto \delta_{\mathbf{k}\mathbf{q}} \delta_{mn} \delta_{\sigma\tau}$ .

LOSC’s localized orbitals are called orbitalets in finite systems [31] and dually localized Wannier functions (DLWFs) in periodic boundary conditions [53]. DLWFs are generalized Wannier functions [54] constructed from the Kohn–Sham Bloch orbitals  $|\psi_{\mathbf{k}n\sigma}\rangle$ , where  $\mathbf{k}$  indexes the  $N_k$  points sampled from the irreducible Brillouin zone,  $n$  the electronic bands, and  $\sigma$  the spin, as

$$|w_{\mathbf{R}i\sigma}\rangle = \frac{1}{N_k} \sum_{\mathbf{k}} e^{-i\mathbf{k}\cdot\mathbf{R}} \sum_n U_{ni}^{\mathbf{k}} |\psi_{\mathbf{k}n\sigma}\rangle. \quad (2)$$

The DLWFs are periodic on a supercell  $N_k$  times larger than the primitive unit cell and are indexed by a band-like index  $i$  and a primitive cell translation vector  $\mathbf{R}$ . At each  $\mathbf{k}$ -point, the unitary operator  $U^{\mathbf{k}}$  is chosen to minimize the cost function

$$F = \sum_i [(1 - \gamma) \Delta r_{\mathbf{0}i\sigma}^2 + \gamma \Delta h_{\mathbf{0}i\sigma}^2], \quad (3)$$

where  $\Delta r_{\mathbf{0}i\sigma}^2$  is the spatial variance  $\langle w_{\mathbf{0}i\sigma} | \mathbf{r} | w_{\mathbf{0}i\sigma} \rangle^2 - \langle w_{\mathbf{0}i\sigma} | r^2 | w_{\mathbf{0}i\sigma} \rangle$  and  $\Delta h_{\mathbf{0}i\sigma}^2$  is the energy variance. The numerical value of  $\gamma$  depends on the units chosen, but all LOSC results to date have used the same value; when  $\Delta r^2$  is computed in  $a_0^2$  and  $\Delta h^2$  in  $\text{eV}^2$ ,  $\gamma = 0.47714$ . (Setting  $\gamma = 0$  recovers maximally localized Wannier functions [55].) Despite being spatially localized, DLWFs

retain information about the energy spectrum, necessary for describing chemical reactivity [56]. DLWFs also extend readily to metals because they combine both the (occupied) valence and (unoccupied) conduction manifolds in their construction. [30, 31, 53].

In finite systems, the curvature is  $\kappa_{nn\sigma} = \partial^2 E / \partial f_{n\sigma}^2$ , where  $f_{n\sigma}$  is the occupation of the Kohn–Sham orbital  $|\psi_{n\sigma}\rangle$ . When  $|\psi_{n\sigma}\rangle$  is a frontier orbital,  $\partial^2 E / \partial f_{n\sigma}^2$  describes the deviation of  $E(N)$ , computed by a DFA, from the correct linear behavior, including the effect of screening by all other electrons (also called orbital relaxation) [38]. The original GSC method approximated  $\kappa_{nn\sigma}$ , treating only the Coulomb interaction, and used Kohn–Sham orbital densities instead of the Fukui function  $\partial \rho_{\sigma} / \partial f_{n\sigma}$  [35, 36]. Yang *et al.* [38] extended the result to include the exchange–correlation interaction, finding the exact second-order derivatives to be

$$\begin{aligned} \kappa_{nn\sigma} &= \langle \rho_{n\sigma} | \sum_{\tau} (\epsilon^{\tau})^{-1} f_{\text{Hxc}}^{\tau\sigma} | \rho_{n\sigma} \rangle \\ &= \langle \rho_{n\sigma} | f_{\text{Hxc}}^{\sigma\sigma} + \sum_{\nu\tau} f_{\text{Hxc}}^{\sigma\nu} \chi^{\nu\tau} f_{\text{Hxc}}^{\tau\sigma} | \rho_{n\sigma} \rangle. \end{aligned} \quad (4)$$

Here,  $\rho_{n\sigma}(\mathbf{r}) = |\psi_{n\sigma}(\mathbf{r})|^2$  is the density of the Kohn–Sham orbital  $|\psi_{n\sigma}\rangle$ ;  $(\epsilon^{\tau})^{-1}(\mathbf{r}, \mathbf{r}')$  is the inverse static microscopic dielectric function;

$$\begin{aligned} f_{\text{Hxc}}^{\sigma\nu}(\mathbf{r}, \mathbf{r}') &= \frac{\delta^2 E_{\text{Hxc}}}{\delta \rho^{\sigma}(\mathbf{r}) \delta \rho^{\nu}(\mathbf{r}')} \\ &= \frac{1}{|\mathbf{r} - \mathbf{r}'|} + \frac{\delta^2 E_{\text{xc}}}{\delta \rho^{\sigma}(\mathbf{r}) \delta \rho^{\nu}(\mathbf{r}')} \end{aligned} \quad (5)$$

is the Hartree–exchange–correlation kernel; and

$$\chi^{\nu\tau}(\mathbf{r}, \mathbf{r}') = \frac{\delta \rho^{\nu}(\mathbf{r})}{\delta v^{\tau}(\mathbf{r}')} = \frac{\delta^2 E}{\delta v^{\nu}(\mathbf{r}) \delta v^{\tau}(\mathbf{r}')} \quad (6)$$

is the response of the density to an external perturbing potential  $\delta v$ , to linear order. Observe that the curvature is given by a bare kernel  $f_{\text{Hxc}}$  screened by the inverse dielectric function  $\epsilon^{-1}$ , or equivalently by the sum of the bare kernel and a relaxed kernel modulated by  $\chi$ . This curvature was implemented in the most recent iteration of GSC, known as GSC2 [37]. Compared to the initial implementation, including orbital relaxation modestly improves the performance of GSC, reducing the error in ionization energy and electron affinity for small molecules by an average of about 0.2 eV. GSC2 still gives no correction to the total energy for materials; its screened interaction must be combined with the localized DLWFs. In molecules, including both the screening of (4) and localization greatly improves the energies of core-orbital quasiparticles [41].

In LOSC, the GSC2 curvature is transformed to the DLWF basis; its matrix elements are

$$\kappa_{\mathbf{R}ij\sigma} = \langle \rho_{\mathbf{0}i\sigma} | f_{\text{Hxc}}^{\sigma\sigma} + \sum_{\nu\tau} f_{\text{Hxc}}^{\sigma\nu} \chi^{\nu\tau} f_{\text{Hxc}}^{\tau\sigma} | \rho_{\mathbf{R}j\sigma} \rangle, \quad (7)$$

where  $\rho_{\mathbf{R}j\sigma}(\mathbf{r}) = |w_{\mathbf{R}j\sigma}(\mathbf{r})|^2$  is a DLWF density. Note that  $\kappa$  in LOSC is not diagonal because the DLWFs are not Kohn–Sham eigenfunctions. These off-diagonal elements allow interactions between pairs of orbitals to affect the total energy, even at long range. The analogous elements for canonical orbitals were derived as cross-terms  $\partial^2 E / \partial f_{n\sigma} \partial f_{m\sigma}$  in the GSC2 method (see the Supporting Information of Mei *et al.* [37]). In lrLOSC, we compute  $\kappa_{\mathbf{R}ij\sigma}$  using density functional perturbation theory [57]; this reduces the computational cost by a factor of  $N_k$ , the number of  $\mathbf{k}$ -points, because both curvature elements linear in DLWF densities [58] and the densities themselves [45] decompose monochromatically. Thus

$$\kappa_{\mathbf{R}ij\sigma} = \frac{1}{N_k} \sum_{\mathbf{q}} e^{-i\mathbf{q}\cdot\mathbf{R}} \times \left[ \langle \rho_{\mathbf{0}i\sigma}^{\mathbf{q}} | V_{\mathbf{0}j\sigma}^{\mathbf{q}} \rangle + \sum_{\tau} \langle \delta\rho_{\mathbf{0}i\tau}^{\mathbf{q}} | V_{\mathbf{0}j\tau}^{\mathbf{q}} \rangle \right], \quad (8)$$

where  $\mathbf{q}$  samples the Brillouin zone uniformly including its origin; and

$$V_{\mathbf{0}j\tau}^{\mathbf{q}}(\mathbf{r}) = \int d\mathbf{r}' f_{\text{Hxc}}^{\tau\sigma}(\mathbf{r}, \mathbf{r}') \rho_{\mathbf{0}j\sigma}^{\mathbf{q}}(\mathbf{r}'), \quad (9)$$

$$\delta\rho_{\mathbf{0}i\tau}^{\mathbf{q}}(\mathbf{r}') = \sum_{\nu} \int d\mathbf{r}'' \chi^{\tau\nu}(\mathbf{r}, \mathbf{r}'') V_{\mathbf{0}i\nu}^{\mathbf{q}}(\mathbf{r}''). \quad (10)$$

See the Supplemental Material for the details of this derivation.[59] Computing  $|\delta\rho_{\mathbf{0}i\tau}^{\mathbf{q}}\rangle$  occupies the vast majority of lrLOSC’s computational time. For each  $|\rho_{\mathbf{0}i\tau}^{\mathbf{q}}\rangle$ , there are  $N_{\text{occ}}$  coupled equations that must be solved at each  $\mathbf{k}$ -point, for a total runtime scaling as  $\mathcal{O}(N_{\text{DLWF}} N_{\mathbf{k}}^2 N_{\text{occ}}^3)$  (since  $N_{\mathbf{q}} = N_{\mathbf{k}}$ ).

lrLOSC greatly improves fundamental gaps relative to PBE. In FIG. 1, we show the band structure of lithium fluoride calculated with PBE (left) and lrLOSC (right). The DFA gap is only 9.19 eV, much smaller than the electronic gap (15.43 eV, including a phonon-mediated zero-point renormalization of  $-1.231$  eV). lrLOSC shifts the occupied bands down and the virtual bands up relative to PBE and predicts a gap of 15.24 eV, within 0.2 eV of the correct gap. lrLOSC also improves the core-level energies, especially the lithium 1s state, compared to the parent DFA. Its performance is very similar in this system to the Koopmans-compliant Wannier functional [45]; it slightly outperforms  $G_0W_0$  in the electronic gap, but is outperformed in turn for the core-level energies.

The lrLOSC band gap correction for silicon carbide is particularly accurate (FIG. 3). The qualitative features of the DFA band gap are virtually unchanged, but the electronic gap is adjusted to within 0.04 eV of the correct value. A modest increase in conduction band energies—coupled with a large downward shift in core-level energies, leaving valence energies mostly unchanged relative to the Fermi level—is typical behavior for lrLOSC on the

systems tested. In the systems tested, however, the lrLOSC Fermi level is always observed to be lower than  $E_F^{\text{PBE}}$ .

Altogether, we have obtained lrLOSC total energies and band structures for a set of thirteen semiconductors and insulators. All but neon and argon have zero-point renormalization (ZPR) corrections available in the literature [62–64], which gives us equal footing to compare the *electronic* (fundamental) contribution to the experimental (optical) band gap to lrLOSC’s prediction. We thus omit Ne and Ar from the quantitative discussion of lrLOSC.

On the remaining eleven materials, the mean absolute error (MAE) in the lrLOSC fundamental gap, relative to the electronic (experimental – ZPR) gap, is 0.28 eV. This result is even better than that from some many-body methods. Equation-of-motion coupled-cluster theory with single and double excitations yields a fundamental gap MAE of 0.42 eV on a similar set of materials [65]. Quasiparticle self-consistent *GW* [66, 67] similarly gives a MAE between 0.4 and 0.6 eV; including vertex corrections improves the performance beyond lrLOSC’s, but at substantial computational cost.

Our DFA calculations are performed with `Quantum ESPRESSO` [68–70], version 7.1. We use the PBE functional [71], optimized norm-conserving Vanderbilt pseudopotentials [72] built under PBE with scalar relativistic corrections, a wavefunction kinetic energy cutoff of 75 Ry, and a  $6 \times 6 \times 6$  Monkhorst–Pack sampling of the irreducible Brillouin zone; the PBE valence band maximum and conduction band minimum is converged to within 0.01 eV. We scale the correction [73] to the Coulomb divergence in  $\langle \delta\rho_{\mathbf{0}i\tau}^{\mathbf{q}} | V_{\mathbf{0}j\tau}^{\mathbf{q}} \rangle$  by the macroscopic dielectric constant  $\epsilon_{\infty}$ ; it is computed in `Quantum ESPRESSO`’s `PHonon` module, with the same parameters, which are sufficient to converge  $\epsilon_{\infty}$  to 0.01.

DLWFs are obtained with a locally maintained fork [53] of `wannier90` [74–76], and lrLOSC is implemented in a local fork of `Quantum ESPRESSO`’s development version. It adapts the `KCW` module [45], leveraging its implementation of the monochromatic decomposition and its linear-response routines.

TABLE I. Theoretical and experimental core-level quasiparticle energies and electronic gap of LiF (all in eV).  $G_0W_0$  is from [60], and uses LDA rather than PBE; Koopmans spectral functional (KI) is from [45]; PBE and lrLOSC are from this work. Experimental core energies are from [61]; the gap is from [18] and containing references, and the zero-point renormalization is computed in [62].

	PBE	$G_0W_0$	KI	lrLOSC	Exp.
Li (1s)	−40.8	−47.2	−46.6	−47.8	−49.8
F (2s)	−19.5	−24.8	−19.5	−19.7	−23.9
$E_g$ – ZPR	9.2	14.3	15.3	15.2	15.4

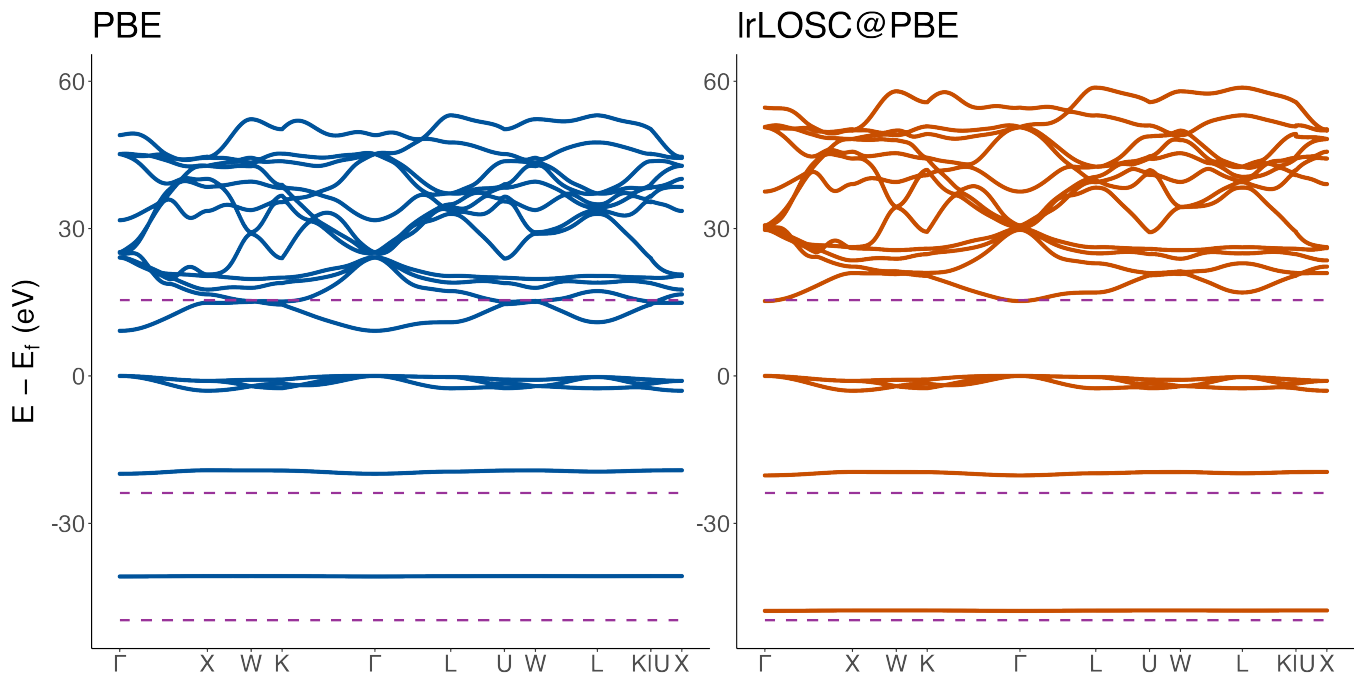


FIG. 1. LiF band structure by PBE and lrLOSC. Purple dashed lines (top to bottom): ZPR-corrected experimental gap, experimental energies for F 2s, Li 1s states.

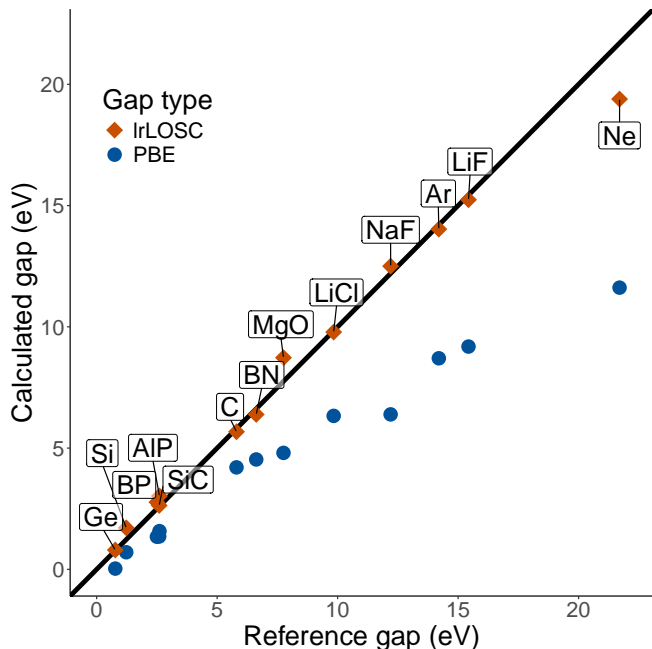


FIG. 2. Fundamental gaps predicted by lrLOSC vs. by PBE. Reference: experimental gaps – zero-point renormalization.

There is only one free parameter,  $\gamma$ , in lrLOSC; it describes the balance between spatial and energy localization of the DLWFs in (3). The value we choose,  $\gamma = 0.47714$ , was originally optimized for LOSC in fi-

nite systems [31]; it is also used for sLOSC in materials [42]. We found that lrLOSC was quite accurate without any further tuning of  $\gamma$ .

Because it includes both localization and system-dependent screening, lrLOSC corrects delocalization error effectively in both molecules and materials. It provides accurate, size-consistent orbital and band energy corrections in semiconductors and insulators, matching the performance of many-body perturbation theory without requiring any many-body observables. In its current implementation, it is limited to gapped systems, although it is in principle extensible to metals using similar techniques to those in density functional perturbation theory [57]. Future work will implement an approximate, but still system-dependent, curvature, improving LOSC’s computational efficiency. We also seek to apply LOSC self-consistently, yielding a correction to the electron density; this feature has already been demonstrated for molecules [77]. With these updates, LOSC will be applicable to interfaces, including molecules on a solid surface. Modeling energy level alignment at interfaces is a major challenge for electronic structure methods [78–80], and lrLOSC promises a nearly parameter-free solution entirely within the confines of DFT.

We thank Yichen Fan and Jincheng Yu for helpful discussions of LOSC in molecules, and gratefully acknowledge funding from the National Science Foundation (CHE-2154831) and National Institutes of Health (5R01GM061870-20).

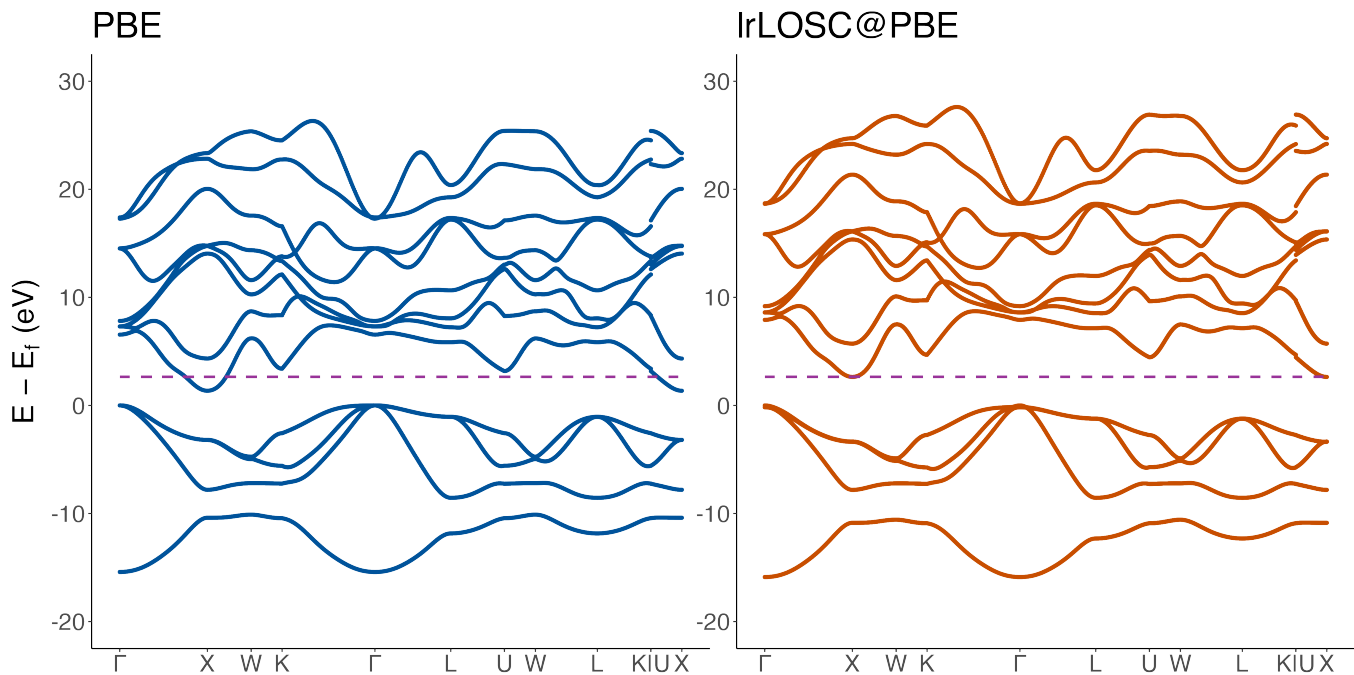


FIG. 3. SiC band structure. Purple dashed line: ZPR-corrected experimental gap.

\* weitao.yang@duke.edu; Department of Physics, Duke University, Durham, NC 27708, USA

- [1] P. Hohenberg and W. Kohn, *Phys. Rev.* **136**, B864 (1964).
- [2] W. Kohn and L. J. Sham, *Phys. Rev.* **140**, A1133 (1965).
- [3] M. Levy, *Proc. Natl. Acad. Sci. U.S.A.* **76**, 6062 (1979).
- [4] M. Levy, *Phys. Rev. A* **26**, 1200 (1982).
- [5] E. H. Lieb, *Int. J. Quantum Chem.* **24**, 243 (1983).
- [6] A. J. Cohen, P. Mori-Sánchez, and W. Yang, *Phys. Rev. B* **77**, 115123 (2008).
- [7] W. Yang, A. J. Cohen, and P. Mori-Sánchez, *J. Chem. Phys.* **136**, 204111 (2012).
- [8] J. F. Janak, *Phys. Rev. B* **18**, 7165 (1978).
- [9] J. P. Perdew, R. G. Parr, M. Levy, and J. L. Balduz, *Phys. Rev. Lett.* **49**, 1691 (1982).
- [10] W. Yang, Y. Zhang, and P. W. Ayers, *Phys. Rev. Lett.* **84**, 5172 (2000).
- [11] J. P. Perdew, *Int. J. Quantum Chem.* **28**, 497 (1985).
- [12] M. S. Hybertsen and S. G. Louie, *Phys. Rev. B* **34**, 5390 (1986).
- [13] I. Dabo, A. Ferretti, N. Poilvert, Y. Li, N. Marzari, and M. Cococcioni, *Phys. Rev. B* **82**, 115121 (2010).
- [14] T. Tsuneda, J.-W. Song, S. Suzuki, and K. Hirao, *J. Chem. Phys.* **133**, 174101 (2010).
- [15] L. Kronik, T. Stein, S. Refaely-Abramson, and R. Baer, *J. Chem. Theory Comput.* **8**, 1515 (2012).
- [16] T. Körzdörfer, R. M. Parrish, N. Marom, J. S. Sears, C. D. Sherrill, and J.-L. Brédas, *Phys. Rev. B* **86**, 205110 (2012).
- [17] P. Puschnig, A. D. Boese, M. Willenbockel, M. Meyer, D. Lüftner, E. M. Reinisch, T. Ules, G. Koller, S. Soubatch, M. G. Ramsey, and F. S. Tautz, *J. Phys. Chem. Lett.* **8**, 208 (2017).
- [18] J. Heyd, J. E. Peralta, G. E. Scuseria, and R. L. Martin, *J. Chem. Phys.* **123**, 174101 (2005).
- [19] H. Xiao, J. Tahir-Kheli, and W. A. I. Goddard, *J. Phys. Chem. Lett.* **2**, 212 (2011).
- [20] S. Wang, T. Sakurai, W. Wen, and Y. Qi, *Adv. Mater. Interfaces* **5**, 1800260 (2018).
- [21] Y. Li, Y.-L. Li, B. Sa, and R. Ahuja, *Catal. Sci. Technol.* **7**, 545 (2017).
- [22] H. Ishii, K. Sugiyama, E. Ito, and K. Seki, *Advanced Materials* **11**, 605 (1999).
- [23] S. Braun, W. R. Salaneck, and M. Fahlman, *Advanced Materials* **21**, 1450 (2009).
- [24] H. Kroemer, *Rev. Mod. Phys.* **73**, 783 (2001).
- [25] *Nature Mater* **11**, 91 (2012).
- [26] P. Mori-Sánchez, A. J. Cohen, and W. Yang, *Phys. Rev. Lett.* **100**, 146401 (2008).
- [27] A. J. Cohen, P. Mori-Sánchez, and W. Yang, *Science* **321**, 792 (2008).
- [28] A. J. Cohen, P. Mori-Sánchez, and W. Yang, *Chem. Rev.* **112**, 289 (2012).
- [29] K. R. Bryenton, A. A. Adeleke, S. G. Dale, and E. R. Johnson, *WIREs Computational Molecular Science* **n/a**, e1631 (2022).
- [30] C. Li, X. Zheng, N. Q. Su, and W. Yang, *Nat. Sci. Rev.* **5**, 203 (2018).
- [31] N. Q. Su, A. Mahler, and W. Yang, *J. Phys. Chem. Lett.* **11**, 1528 (2020).
- [32] Y. Mei, N. Yang, and W. Yang, *J. Chem. Phys.* **154**, 054302 (2021).
- [33] Y. Mei, C. Li, N. Q. Su, and W. Yang, *J. Phys. Chem. A* **123**, 666 (2019).
- [34] J. Li, Y. Jin, N. Q. Su, and W. Yang, *J. Chem. Phys.*

- 156**, 154101 (2022).
- [35] X. Zheng, A. J. Cohen, P. Mori-Sánchez, X. Hu, and W. Yang, *Phys. Rev. Lett.* **107**, 026403 (2011).
- [36] D. Zhang, X. Zheng, C. Li, and W. Yang, *J. Chem. Phys.* **142**, 154113 (2015).
- [37] Y. Mei, Z. Chen, and W. Yang, *J. Phys. Chem. Lett.* **12**, 7236 (2021).
- [38] W. Yang, A. J. Cohen, F. De Proft, and P. Geerlings, *J. Chem. Phys.* **136**, 144110 (2012).
- [39] D. Zhang, X. Yang, X. Zheng, and W. Yang, *Molecular Physics* **116**, 927 (2018).
- [40] X. Yang, X. Zheng, and W. Yang, *Front. Chem.* **8** (2020).
- [41] J. Yu, Y. Mei, Z. Chen, and W. Yang, Accurate Prediction of Core Level Binding Energies from Ground-State Density Functional Calculations: The Importance of Localization and Screening (2024), arXiv:2406.06345 [physics].
- [42] A. Mahler, J. Williams, N. Q. Su, and W. Yang, *Phys. Rev. B* **106**, 035147 (2022).
- [43] N. L. Nguyen, N. Colonna, A. Ferretti, and N. Marzari, *Phys. Rev. X* **8**, 021051 (2018).
- [44] N. Colonna, N. L. Nguyen, A. Ferretti, and N. Marzari, *J. Chem. Theory Comput.* **14**, 2549 (2018).
- [45] N. Colonna, R. De Gennaro, E. Linscott, and N. Marzari, *J. Chem. Theory Comput.* **18**, 5435 (2022).
- [46] J. Ma and L.-W. Wang, *Sci. Rep.* **6**, 24924 (2016).
- [47] M. Weng, S. Li, J. Ma, J. Zheng, F. Pan, and L.-W. Wang, *Applied Physics Letters* **111**, 054101 (2017).
- [48] S. Li, M. Weng, J. Jie, J. Zheng, F. Pan, and L.-W. Wang, *EPL* **123**, 37002 (2018).
- [49] M. Weng, S. Li, J. Zheng, F. Pan, and L.-W. Wang, *J. Phys. Chem. Lett.* **9**, 281 (2018).
- [50] M. Weng, F. Pan, and L.-W. Wang, *npj Comput Mater* **6**, 1 (2020).
- [51] D. Wing, G. Ohad, J. B. Haber, M. R. Filip, S. E. Gant, J. B. Neaton, and L. Kronik, *Proc Natl Acad Sci USA* **118**, e2104556118 (2021).
- [52] G. Ohad, D. Wing, S. E. Gant, A. V. Cohen, J. B. Haber, F. Sagredo, M. R. Filip, J. B. Neaton, and L. Kronik, *Phys. Rev. Mater.* **6**, 104606 (2022).
- [53] A. Mahler, J. Z. Williams, N. Q. Su, and W. Yang, Wannier Functions Dually Localized in Space and Energy (2022), arXiv:2201.07751v1 [cond-mat.mtrl-sci].
- [54] G. H. Wannier, *Phys. Rev.* **52**, 191 (1937).
- [55] N. Marzari and D. Vanderbilt, *Phys. Rev. B* **56**, 12847 (1997).
- [56] J. Yu, N. Q. Su, and W. Yang, *JACS Au* **2**, 1383 (2022).
- [57] S. Baroni, S. de Gironcoli, A. Dal Corso, and P. Giannozzi, *Rev. Mod. Phys.* **73**, 515 (2001).
- [58] I. Timrov, N. Marzari, and M. Cococcioni, *Phys. Rev. B* **98**, 085127 (2018).
- [59] See Supplemental Material at [URL will be inserted by publisher] for details on the monochromatic decomposition of the curvature; a note on symmetry and degeneracy; the unit-cell periodicity of  $\kappa$ ; and the data underlying FIG. 2. It also contains references [81–86].
- [60] N.-P. Wang, M. Rohlfing, P. Krüger, and J. Pollmann, *Phys. Rev. B* **67**, 115111 (2003).
- [61] L. I. Johansson and S. B. M. Hagström, *Phys. Scr.* **14**, 55 (1976).
- [62] M. Engel, H. Miranda, L. Chaput, A. Togo, C. Verdi, M. Marsman, and G. Kresse, *Phys. Rev. B* **106**, 094316 (2022).
- [63] A. Miglio, V. Brousseau-Couture, E. Godbout, G. Antoinius, Y.-H. Chan, S. G. Louie, M. Côté, M. Giantomassi, and X. Gonze, *npj Comput Mater* **6**, 1 (2020).
- [64] H. Shang, J. Zhao, and J. Yang, *J. Phys. Chem. C* **125**, 6479 (2021).
- [65] E. A. Vo, X. Wang, and T. C. Berkelbach, *The Journal of Chemical Physics* **160**, 044106 (2024).
- [66] W. Chen and A. Pasquarello, *Phys. Rev. B* **92**, 041115 (2015).
- [67] J. Lei and T. Zhu, *J. Chem. Phys.* **157**, 214114 (2022).
- [68] P. Giannozzi, S. Baroni, N. Bonini, M. Calandra, R. Car, C. Cavazzoni, D. Ceresoli, G. L. Chiarotti, M. Cococcioni, I. Dabo, A. Dal Corso, S. de Gironcoli, S. Fabris, G. Fratesi, R. Gebauer, U. Gerstmann, C. Gougoussis, A. Kokalj, M. Lazzeri, L. Martin-Samos, N. Marzari, F. Mauri, R. Mazzarello, S. Paolini, A. Pasquarello, L. Paulatto, C. Sbraccia, S. Scandolo, G. Sclauzero, A. P. Seitsonen, A. Smogunov, P. Umari, and R. M. Wentzcovitch, *J. Phys.: Condens. Matter* **21**, 395502 (2009).
- [69] P. Giannozzi, O. Andreussi, T. Brumme, O. Bunau, M. Buongiorno Nardelli, M. Calandra, R. Car, C. Cavazzoni, D. Ceresoli, M. Cococcioni, N. Colonna, I. Carnimeo, A. Dal Corso, S. de Gironcoli, P. Delugas, R. A. DiStasio, A. Ferretti, A. Floris, G. Fratesi, G. Fugallo, R. Gebauer, U. Gerstmann, F. Giustino, T. Gorni, J. Jia, M. Kawamura, H.-Y. Ko, A. Kokalj, E. Küçükbenli, M. Lazzeri, M. Marsili, N. Marzari, F. Mauri, N. L. Nguyen, H.-V. Nguyen, A. Otero-de-la-Roza, L. Paulatto, S. Poncé, D. Rocca, R. Sabatini, B. Santra, M. Schlipf, A. P. Seitsonen, A. Smogunov, I. Timrov, T. Thonhauser, P. Umari, N. Vast, X. Wu, and S. Baroni, *J. Phys.: Condens. Matter* **29**, 465901 (2017).
- [70] P. Giannozzi, O. Baseggio, P. Bonfà, D. Brunato, R. Car, I. Carnimeo, C. Cavazzoni, S. de Gironcoli, P. Delugas, F. Ferrari Ruffino, A. Ferretti, N. Marzari, I. Timrov, A. Urru, and S. Baroni, *J. Chem. Phys.* **152**, 154105 (2020).
- [71] J. P. Perdew, K. Burke, and M. Ernzerhof, *Phys. Rev. Lett.* **77**, 3865 (1996).
- [72] D. R. Hamann, *Phys. Rev. B* **88**, 085117 (2013).
- [73] F. Gygi and A. Baldereschi, *Phys. Rev. B* **34**, 4405 (1986).
- [74] A. A. Mostofi, J. R. Yates, Y.-S. Lee, I. Souza, D. Vanderbilt, and N. Marzari, *Computer Physics Communications* **178**, 685 (2008).
- [75] A. A. Mostofi, J. R. Yates, G. Pizzi, Y.-S. Lee, I. Souza, D. Vanderbilt, and N. Marzari, *Computer Physics Communications* **185**, 2309 (2014).
- [76] G. Pizzi, V. Vitale, R. Arita, S. Blügel, F. Freimuth, G. Géranton, M. Gibertini, D. Gresch, C. Johnson, T. Koretsune, J. Ibañez-Azpiroz, H. Lee, J.-M. Lihm, D. Marchand, A. Marrazzo, Y. Mokrousov, J. I. Mustafa, Y. Nohara, Y. Nomura, L. Paulatto, S. Poncé, T. Ponweiser, J. Qiao, F. Thöle, S. S. Tsirkin, M. Wierzbowska, N. Marzari, D. Vanderbilt, I. Souza, A. A. Mostofi, and J. R. Yates, *J. Phys.: Condens. Matter* **32**, 165902 (2020).
- [77] Y. Mei, Z. Chen, and W. Yang, *J. Phys. Chem. Lett.* **11**, 10269 (2020).
- [78] F. Flores, J. Ortega, and H. Vázquez, *Phys. Chem. Chem. Phys.* **11**, 8658 (2009).
- [79] D. A. Egger, Z.-F. Liu, J. B. Neaton, and L. Kronik, *Nano Lett.* **15**, 2448 (2015).
- [80] Z.-F. Liu, *J. Chem. Phys.* **152**, 054103 (2020).

- [81] H. J. Monkhorst and J. D. Pack, Phys. Rev. B **13**, 5188 (1976).
- [82] C. A. Rozzi, D. Varsano, A. Marini, E. K. U. Gross, and A. Rubio, Phys. Rev. B **73**, 205119 (2006).
- [83] G. J. Martyna and M. E. Tuckerman, The Journal of Chemical Physics **110**, 2810 (1999).
- [84] Ralph. W. G. Wyckoff, *Crystal Structures*, 2nd ed. (Wiley, New York, 1973).
- [85] F. Tran and P. Blaha, Phys. Rev. Lett. **102**, 226401 (2009).
- [86] R. T. Poole, J. G. Jenkin, J. Liesegang, and R. C. G. Leckey, Phys. Rev. B **11**, 5179 (1975).

# Supplemental Material: Localized Orbital Scaling Correction with Linear Response in Materials

Jacob Z. Williams and Weitao Yang\*

*Department of Chemistry, Duke University, Durham, NC 27708, USA<sup>†</sup>*

(Dated: July 3, 2024)

## MONOCHROMATIC IMPLEMENTATION OF THE CURVATURE

The second derivative of the Kohn–Sham total energy with respect to the occupation of the canonical orbitals has matrix elements [1, 2]

$$\frac{\partial^2 E}{\partial f_{n\sigma}^2} = \kappa_{nn}^\sigma = \langle \rho_{n\sigma} | f_{\text{Hxc}}^{\sigma\sigma} + \sum_{\nu\tau} f_{\text{Hxc}}^{\sigma\nu} \chi^{\nu\tau} f_{\text{Hxc}}^{\tau\sigma} | \rho_{n\sigma} \rangle. \quad (1)$$

Here,  $f_{n\sigma}$  is the occupation of the canonical orbital  $|\psi_{n\sigma}\rangle$ ;  $\rho_{n\sigma}(\mathbf{r}) = |\psi_{n\sigma}(\mathbf{r})|^2$  is its density;

$$f_{\text{Hxc}}^{\sigma\tau}(\mathbf{r}, \mathbf{r}') = \frac{\delta^2 E_{\text{Hxc}}}{\delta \rho^\sigma(\mathbf{r}) \delta \rho^\tau(\mathbf{r}')} = \frac{1}{|\mathbf{r} - \mathbf{r}'|} + \frac{\delta^2 E_{\text{xc}}}{\delta \rho^\sigma(\mathbf{r}) \delta \rho^\tau(\mathbf{r}')} \quad (2)$$

is the Hartree–exchange–correlation kernel; and

$$\chi^{\nu\tau}(\mathbf{r}, \mathbf{r}') = \frac{\delta \rho^\nu(\mathbf{r})}{\delta v^\tau(\mathbf{r}')} = \frac{\delta^2 E}{\delta v^\nu(\mathbf{r}) \delta v^\tau(\mathbf{r}')} \quad (3)$$

is the density–density response function, which encodes screening. We assume that the Kohn–Sham functional is semilocal for compactness of notation.

We express  $\kappa_\sigma$  in the basis of DLWFs to apply it to LOSC. Its matrix elements become

$$\kappa_{\mathbf{R}ij}^\sigma = \langle \rho_{\mathbf{0}i\sigma} | f_{\text{Hxc}}^{\sigma\sigma} + \sum_{\nu\tau} f_{\text{Hxc}}^{\sigma\nu} \chi^{\nu\tau} f_{\text{Hxc}}^{\tau\sigma} | \rho_{\mathbf{R}j\sigma} \rangle. \quad (4)$$

To simplify this, define  $|V_{\mathbf{R}j\tau}\rangle$  and  $|\delta\rho_{\mathbf{0}i\tau}\rangle$  by

$$\begin{aligned} V_{\mathbf{R}j\tau}(\mathbf{r}) &= \int d\mathbf{r}' f_{\text{Hxc}}^{\tau\sigma}(\mathbf{r}, \mathbf{r}') \rho_{\mathbf{R}j\sigma}(\mathbf{r}'); \\ \delta\rho_{\mathbf{0}i\tau}(\mathbf{r}) &= \sum_\nu \int d\mathbf{r}' \chi^{\tau\nu}(\mathbf{r}, \mathbf{r}') V_{\mathbf{0}i\nu}^\nu(\mathbf{r}') = \sum_\nu \int d\mathbf{r}' \chi^{\tau\nu}(\mathbf{r}, \mathbf{r}') \int d\mathbf{r}'' f_{\text{Hxc}}^{\nu\sigma}(\mathbf{r}', \mathbf{r}'') \rho_{\mathbf{0}i\sigma}(\mathbf{r}''); \end{aligned} \quad (5)$$

then

$$\kappa_{\mathbf{R}ij}^\sigma = \langle \rho_{\mathbf{0}i\sigma} | V_{\mathbf{R}j\sigma} \rangle + \sum_\tau \langle \delta\rho_{\mathbf{0}i\tau} | V_{\mathbf{R}j\tau} \rangle. \quad (6)$$

(Note that  $\sigma$  is a fixed spin index, while  $\tau$  and  $\nu$  vary.)

We call  $|V_{\mathbf{R}j\sigma}\rangle$  the bare potential from DLWF  $|\rho_{\mathbf{R}j\sigma}\rangle$  and  $|\delta\rho_{\mathbf{0}i\tau}\rangle$  the screened response of  $|\rho_{\mathbf{0}i\sigma}\rangle$  to  $|V_{\mathbf{0}i\tau}\rangle$ .



## The monochromatic decomposition

Linear-response quantities in periodic boundary conditions are expressible as a sum over crystal momentum vectors  $\mathbf{q}$ . If the Brillouin zone is uniformly sampled by a Monkhorst–Pack mesh [3], the  $\mathbf{q}$ -points decouple from one another; in the language of density functional perturbation theory, only *monochromatic* (i.e., single- $\mathbf{q}$ ) perturbations need be considered [4]. Timrov *et al.* [5] leveraged this feature in the context of DFT+ $U$ , monochromatically decomposing the linear-response formulation of the Hubbard parameter. More recently, Colonna *et al.* [6] found that Wannier function densities—including DLWF densities  $|\rho_{\mathbf{R}i\sigma}\rangle$ —also decompose monochromatically. This derivation follows their work. At the risk of abuse of notation, we alternate rather freely between states like  $|\rho_{\mathbf{R}i\sigma}\rangle$  and their real-space representations  $\rho_{\mathbf{R}i\sigma}(\mathbf{r}) = \langle \mathbf{r} | \rho_{\mathbf{R}i\sigma} \rangle$ .

Assuming identical Monkhorst–Pack meshes  $\{\mathbf{k}\}$  and  $\{\mathbf{q}\}$ , both centered at the origin  $\Gamma$  of the Brillouin zone, and using  $z^*$  for the complex conjugate of  $z$ , we may write

$$\begin{aligned}
\rho_{\mathbf{R}i\sigma}(\mathbf{r}) &= |w_{\mathbf{R}i\sigma}(\mathbf{r})|^2 = \frac{1}{N_k^2} \left( \sum_{\mathbf{k}} e^{+i\mathbf{k}\cdot\mathbf{R}} \phi_{\mathbf{k}i\sigma}^*(\mathbf{r}) \right) \left( \sum_{\mathbf{q}} e^{-i\mathbf{q}\cdot\mathbf{R}} \phi_{\mathbf{q}i\sigma}(\mathbf{r}) \right) \\
&= \frac{1}{N_k^2} \left[ \sum_{\mathbf{k}} e^{i\mathbf{k}\cdot\mathbf{R}} (e^{-i\mathbf{k}\cdot\mathbf{r}} \phi_{\mathbf{k}i\sigma}^*(\mathbf{r})) \right] \times \left[ \sum_{\mathbf{q}} e^{-i\mathbf{q}\cdot\mathbf{R}} (e^{i\mathbf{q}\cdot\mathbf{r}} \phi_{\mathbf{q}i\sigma}(\mathbf{r})) \right] \\
&= \frac{1}{N_k^2} \sum_{\mathbf{k}} \sum_{\mathbf{q}} e^{i\mathbf{k}\cdot\mathbf{R}} e^{-i\mathbf{q}\cdot\mathbf{R}} e^{-i\mathbf{k}\cdot\mathbf{r}} e^{i\mathbf{q}\cdot\mathbf{r}} \phi_{\mathbf{k}i\sigma}^*(\mathbf{r}) \phi_{\mathbf{q}i\sigma}(\mathbf{r}) \\
&= \frac{1}{N_k} \sum_{\mathbf{q}} e^{i\mathbf{q}\cdot\mathbf{r}} \left[ e^{-i\mathbf{q}\cdot\mathbf{R}} \times \frac{1}{N_k} \sum_{\mathbf{k}} e^{i\mathbf{k}\cdot\mathbf{R}} e^{-i\mathbf{k}\cdot\mathbf{r}} \phi_{\mathbf{k}i\sigma}^*(\mathbf{r}) \phi_{\mathbf{q}i\sigma}(\mathbf{r}) \right].
\end{aligned} \tag{7}$$

The orbitals  $|\phi_{\mathbf{k}i\sigma}\rangle = \sum_n U_{ni}^{\mathbf{k}} |\psi_{\mathbf{k}n\sigma}\rangle$  are unitary transforms of the Kohn–Sham orbitals, without the Fourier transform that makes them Wannier functions. Relabeling  $\mathbf{q} \mapsto \mathbf{k} + \mathbf{q}$  only reorders terms in  $\sum_{\mathbf{q}}$ , and we have

$$\begin{aligned}
\rho_{\mathbf{R}i\sigma}(\mathbf{r}) &= \frac{1}{N_k} \sum_{\mathbf{q}} e^{i(\mathbf{k}+\mathbf{q})\cdot\mathbf{r}} \left[ e^{-i(\mathbf{k}+\mathbf{q})\cdot\mathbf{R}} \times \frac{1}{N_k} (e^{i\mathbf{k}\cdot\mathbf{R}} e^{-i\mathbf{k}\cdot\mathbf{r}} \phi_{\mathbf{k}i\sigma}^*(\mathbf{r}) \phi_{(\mathbf{k}+\mathbf{q})i\sigma}(\mathbf{r})) \right] \\
&= \frac{1}{N_k} \sum_{\mathbf{q}} e^{i\mathbf{q}\cdot\mathbf{r}} \left[ e^{-i\mathbf{q}\cdot\mathbf{R}} \frac{1}{N_k} \sum_{\mathbf{k}} e^{i\mathbf{k}\cdot\mathbf{R}} e^{-i\mathbf{k}\cdot\mathbf{r}} e^{-i\mathbf{k}\cdot\mathbf{r}} e^{i\mathbf{k}\cdot\mathbf{r}} \phi_{\mathbf{k}i\sigma}^*(\mathbf{r}) \phi_{(\mathbf{k}+\mathbf{q})i\sigma}(\mathbf{r}) \right] \\
&= \frac{1}{N_k} \sum_{\mathbf{q}} e^{i\mathbf{q}\cdot\mathbf{r}} \left[ e^{-i\mathbf{q}\cdot\mathbf{R}} \times \frac{1}{N_k} \sum_{\mathbf{k}} \phi_{\mathbf{k}i\sigma}^*(\mathbf{r}) \phi_{(\mathbf{k}+\mathbf{q})i\sigma}(\mathbf{r}) \right] \\
&:= \frac{1}{N_k} \sum_{\mathbf{q}} e^{i\mathbf{q}\cdot\mathbf{r}} \rho_{\mathbf{R}i\sigma}^{\mathbf{q}}(\mathbf{r}) = \frac{1}{N_k} \sum_{\mathbf{q}} e^{i\mathbf{q}\cdot\mathbf{r}} e^{-i\mathbf{q}\cdot\mathbf{R}} \rho_{\mathbf{0}i\sigma}^{\mathbf{q}}(\mathbf{r}).
\end{aligned} \tag{8}$$

The quantities  $|\rho_{\mathbf{0}i\sigma}^{\mathbf{q}}\rangle$  are periodic on the primitive cell. Additionally, note from the final line that the unit cell translation index  $\mathbf{R}$  of  $|\rho_{\mathbf{R}i}\rangle$  enters into the sum only as a phase; only  $|\rho_{\mathbf{0}i}^{\mathbf{q}}\rangle$  need ever be computed explicitly.

The monochromatic decomposition extends to  $|V_{\mathbf{R}j\tau}\rangle$  and  $|\delta\rho_{\mathbf{0}i\tau}\rangle$ , since

$$\begin{aligned} V_{\mathbf{R}j\tau}(\mathbf{r}) &= \int d\mathbf{r}' f_{\text{Hxc}}^{\tau\sigma}(\mathbf{r}, \mathbf{r}') \rho_{\mathbf{R}j\sigma}(\mathbf{r}') \\ &= \frac{1}{N_k} \sum_{\mathbf{q}} e^{i\mathbf{q}\cdot\mathbf{r}} e^{-i\mathbf{q}\cdot\mathbf{R}} \int d\mathbf{r}' f_{\text{Hxc}}^{\tau\sigma}(\mathbf{r}, \mathbf{r}') \rho_{\mathbf{0}j\sigma}^{\mathbf{q}}(\mathbf{r}') \\ &= \frac{1}{N_k} \sum_{\mathbf{q}} e^{i\mathbf{q}\cdot\mathbf{r}} e^{-i\mathbf{q}\cdot\mathbf{R}} V_{\mathbf{0}j\tau}^{\mathbf{q}}(\mathbf{r}) \end{aligned} \quad (9)$$

and

$$\begin{aligned} \delta\rho_{\mathbf{0}i\tau}(\mathbf{r}) &= \sum_{\nu} \int d\mathbf{r}' \chi^{\tau\nu}(\mathbf{r}, \mathbf{r}') V_{\mathbf{0}j\nu}(\mathbf{r}') \\ &= \frac{1}{N_k} \sum_{\nu} \int d\mathbf{r}' \chi^{\tau\nu}(\mathbf{r}, \mathbf{r}') \sum_{\mathbf{q}} e^{i\mathbf{q}\cdot\mathbf{r}'} V_{\mathbf{0}i\nu}^{\mathbf{q}}(\mathbf{r}') \\ &= \frac{1}{N_k} \sum_{\mathbf{q}} e^{i\mathbf{q}\cdot\mathbf{r}} \sum_{\nu} \int d\mathbf{r}' e^{-i\mathbf{q}\cdot(\mathbf{r}'-\mathbf{r})} \chi^{\tau\nu}(\mathbf{r}, \mathbf{r}') V_{\mathbf{0}i\nu}^{\mathbf{q}}(\mathbf{r}') \\ &= \frac{1}{N_k} \sum_{\mathbf{q}} e^{i\mathbf{q}\cdot\mathbf{r}} \sum_{\nu} \int d\mathbf{r}' \chi^{\tau\nu;\mathbf{q}}(\mathbf{r}, \mathbf{r}') V_{\mathbf{0}i\nu}^{\mathbf{q}}(\mathbf{r}') \\ &= \frac{1}{N_k} \sum_{\mathbf{q}} e^{i\mathbf{q}\cdot\mathbf{r}} \delta\rho_{\mathbf{0}i\tau}^{\mathbf{q}}(\mathbf{r}). \end{aligned} \quad (10)$$

When decomposing  $|V_{\mathbf{R}j\tau}\rangle$ , we used the fact that  $f_{\text{Hxc}}^{\tau\sigma}$  is periodic on the primitive cell, and for  $|\delta\rho_{\mathbf{0}i\tau}\rangle$  we used that

$$\chi^{\tau\nu}(\mathbf{r}, \mathbf{r}') = \sum_{\mathbf{q}} e^{i\mathbf{q}\cdot(\mathbf{r}'-\mathbf{r})} \chi^{\tau\nu;\mathbf{q}}(\mathbf{r}, \mathbf{r}'). \quad (11)$$

Thus, we obtain at last that

$$\kappa_{\mathbf{R}ij}^{\sigma} = \frac{1}{N_k} \sum_{\mathbf{q}} e^{-i\mathbf{q}\cdot\mathbf{R}} \left[ \langle \rho_{\mathbf{0}i\sigma}^{\mathbf{q}} | V_{\mathbf{0}j\sigma}^{\mathbf{q}} \rangle + \sum_{\tau} \langle \delta\rho_{\mathbf{0}i\tau}^{\mathbf{q}} | V_{\mathbf{0}j\tau}^{\mathbf{q}} \rangle \right]. \quad (12)$$

In practice,  $|\delta\rho_{\mathbf{0}i\tau}^{\mathbf{q}}\rangle$  is computed iteratively, instead of evaluating  $\chi^{\tau\nu}$  directly. Extending a standard result in perturbation theory [4], we have that

$$\delta\rho_{\mathbf{0}i\tau}^{\mathbf{q}}(\mathbf{r}) = \sum_{\mathbf{k}} \sum_{n \in \text{occ}} \psi_{\mathbf{k}n\tau}^*(\mathbf{r}) \delta\psi_{(\mathbf{k}+\mathbf{q})n\tau}(\mathbf{r}) + \text{c.c.}, \quad (13)$$

where

$$\delta\psi_{\mathbf{k}n\tau}(\mathbf{r}) = \sum_{m \neq n} \psi_{\mathbf{k}m\tau}(\mathbf{r}) \frac{\langle \psi_{\mathbf{k}m\tau} | \delta V^{\tau} | \psi_{\mathbf{k}n\tau} \rangle}{\varepsilon_{\mathbf{k}n\tau} - \varepsilon_{\mathbf{k}m\tau}} \quad (14)$$

is the linear variation in the Kohn–Sham orbital  $|\psi_{\mathbf{k}n\tau}\rangle$  under the perturbing potential  $\delta V^\tau$ . Computing  $|\delta\psi_{\mathbf{k}n\tau}\rangle$  by Table 14 requires a double sum over both occupied and unoccupied orbitals, which is very expensive; however, it is known [4] that perturbations including only occupied orbitals do not contribute to the density variation. The iterative Sternheimer equations, one for each  $\mathbf{k}$ -point and spin index, yield the variations  $|\delta\psi_{(\mathbf{k}+\mathbf{q})n\tau}\rangle$  in the occupied orbitals as solutions to

$$[h^\tau + \gamma P_{\text{occ}}^{(\mathbf{k}+\mathbf{q})\tau} - \varepsilon_{\mathbf{k}n\tau}] \delta\psi_{(\mathbf{k}+\mathbf{q})n\tau}(\mathbf{r}) = -P_{\text{vir}}^{(\mathbf{k}+\mathbf{q})\tau} [V_{\mathbf{0}i\tau}^{\mathbf{q}}(\mathbf{r}) + \delta V_{\mathbf{0}i\tau}^{\mathbf{q}}(\mathbf{r})] \psi_{\mathbf{k}n\tau}(\mathbf{r}). \quad (15)$$

In (15),  $P_{\text{occ}}^{\mathbf{k}\tau}$  is the projector onto the occupied Kohn–Sham states with spin  $\tau$  at  $\mathbf{k}$ ; likewise,  $P_{\text{vir}}^{\mathbf{k}\tau} = I - P_{\text{occ}}^{\mathbf{k}\tau}$  is the projector onto the virtual states (it’s used as an orthogonalizer). The small, positive real number  $\gamma$  serves as a preconditioner, and the potential response

$$\delta V_{\mathbf{0}i\tau}^{\mathbf{q}}(\mathbf{r}) = \sum_{\zeta} \int d\mathbf{r}' f_{\text{Hxc}}^{\tau\zeta}(\mathbf{r}, \mathbf{r}') \delta\rho_{\mathbf{0}i\zeta}^{\mathbf{q}}(\mathbf{r}') \quad (16)$$

is updated at each iteration. Eqs. (13), (15), and (16) provide a self-consistent cycle for obtaining  $|\delta\rho_{\mathbf{0}i\tau}^{\mathbf{q}}\rangle$ , from which the LOSC curvature is obtained.

The purpose of the monochromatic decomposition is computational savings. Computing  $|\delta\rho_{\mathbf{0}i}\rangle$  naïvely scales as  $(N_e N_k)^3$ , while calculating each  $|\delta\rho_{\mathbf{0}i\sigma}^{\mathbf{q}}\rangle$  scale as  $N_k N_e^3$ ; since there are  $N_k$  of them, a factor of  $N_k$  is saved overall. As the linear-response computation is still quite expensive, this is a significant time savings. For the systems tested in this work,  $N_k = 216$ , so computing lrLOSC on the large supercell would require roughly two orders of magnitude more computational effort.

### Monochromatic implementation of sLOSC curvature

LOSC initially approximated the curvature as

$$\begin{aligned} \kappa_{\mathbf{R}ij}^\sigma(\beta) &= J_{\mathbf{R}ij} + \beta X_{\mathbf{R}ij}^\sigma \\ &= \iint d\mathbf{r} d\mathbf{r}' \frac{\rho_{\mathbf{0}i\sigma}(\mathbf{r}) \rho_{\mathbf{R}j\sigma}(\mathbf{r}')}{|\mathbf{r} - \mathbf{r}'|} + \beta \int d\mathbf{r} C_X [\rho_{\mathbf{0}i\sigma}(\mathbf{r}) \rho_{\mathbf{R}j\sigma}(\mathbf{r})]^{2/3}, \end{aligned} \quad (17)$$

where  $\beta = 6(1 - 1/\sqrt[3]{2})$  is chosen so that the self-exchange in any one-electron density is twice that of the same density with half an electron.  $C_X = 0.75\sqrt[3]{6/\pi}$  is the Dirac exchange constant [7, 8].

This curvature corrects delocalization error in small molecules effectively, but the screening of the Coulomb repulsion by lattice electrons means that it overcorrects band energies in materials severely. The first attempt to improve this behavior, called sLOSC [9], attenuated  $J_{\mathbf{R}ij}^\sigma$  empirically using a complementary error function, replacing the long-range  $1/r$  behavior of the bare Hartree interaction by the exponentially decaying  $\text{erfc}(\alpha r)/r$ . The matrix elements of the sLOSC curvature are

$$\begin{aligned} \kappa_{\mathbf{R}ij}^\sigma(\alpha, \beta) &= J_{\mathbf{R}ij}^\sigma(\alpha) + \beta X_{\mathbf{R}ij}^\sigma \\ &= \iint d\mathbf{r} d\mathbf{r}' \frac{\rho_{\mathbf{0}i\sigma}(\mathbf{r}) \text{erfc}(\alpha|\mathbf{r} - \mathbf{r}'|) \rho_{\mathbf{R}j\sigma}(\mathbf{r}')}{|\mathbf{r} - \mathbf{r}'|} + \beta \int d\mathbf{r} C_X [\rho_{\mathbf{0}i\sigma}(\mathbf{r}) \rho_{\mathbf{R}j\sigma}(\mathbf{r})]^{2/3}, \end{aligned} \quad (18)$$

with the same  $\beta, C_X$  as above;  $\alpha = 0.15 \text{ \AA}^{-1}$  was fit from a dataset of semiconductors and insulators.

However, the sLOSC curvature cannot be decomposed monochromatically because the exchange term  $X_{\mathbf{R}ij}^\sigma$  is not linear in  $|\rho_{\mathbf{R}i\sigma}\rangle$ . In order to apply the monochromatic decomposition to the sLOSC curvature, we replace the Dirac-type exchange  $X$  by the exchange-correlation kernel  $f_{xc}^{\sigma\sigma} = \delta^2 E_{xc} / \delta\rho^\sigma \delta\rho^\sigma$ , obtaining the modified sLOSC curvature

$$\kappa_{\mathbf{R}ij}^\sigma(\alpha, \beta) = \langle \rho_{\mathbf{0}i\sigma} | \frac{\text{erfc}(\alpha|\mathbf{r} - \mathbf{r}'|)}{|\mathbf{r} - \mathbf{r}'|} + \beta f_{xc}^{\sigma\sigma} | \rho_{\mathbf{R}j\sigma} \rangle = \langle \rho_{\mathbf{0}i\sigma} | \tilde{f}_{\text{Hxc}}^{\sigma\sigma}(\alpha, \beta) | \rho_{\mathbf{R}j\sigma} \rangle. \quad (19)$$

This expression can be decomposed monochromatically, as the  $\text{erfc}$ -modified Coulomb kernel and the xc kernel scaled by  $\beta$  remain linear in the DLWF densities. The parameters  $\alpha$  and  $\beta$  must be reset empirically, which is beyond the scope of this work, but the (modified) sLOSC curvature is thus unified with the lrLOSC curvature. The implementation of the sLOSC curvature is very simple: modify  $f_{\text{Hxc}}$  to include the attenuated Coulomb and scaled xc interactions, and set  $|\delta\rho_{\mathbf{0}i\tau}\rangle = 0$ .

Finally, we note that the curvature of sLOSC (and of its predecessor, LOSC2 [8]) are modified by a smoothing error function,

$$\tilde{\kappa}_{\mathbf{R}ij}^\sigma(\alpha, \beta) = \text{erf}(8S_{\mathbf{R}ij}^\sigma) \sqrt{\kappa_{ii\mathbf{0}}^\sigma \kappa_{jj\mathbf{0}}^\sigma} + \text{erfc}(8S_{\mathbf{R}ij}^\sigma) \kappa_{\mathbf{R}ij}^\sigma, \quad (20)$$

where  $S_{\mathbf{R}ij}^\sigma$  is the overlap

$$S_{\mathbf{R}ij}^\sigma = \int d\mathbf{r} [\rho_{\mathbf{0}i\sigma}(\mathbf{r}) \rho_{\mathbf{R}j\sigma}(\mathbf{r})]^{1/2}. \quad (21)$$

$S_{\mathbf{R}ij}^\sigma$  is also nonlinear in  $|\rho_{\mathbf{R}i\sigma}\rangle$ ; to apply the curvature smoothing monochromatically, we could use instead the modified overlap

$$\tilde{S}_{\mathbf{R}ij}^\sigma = \left[ \int d\mathbf{r} \rho_{\mathbf{0}i\sigma}(\mathbf{r}) \rho_{\mathbf{R}j\sigma}(\mathbf{r}) \right]^{1/2}. \quad (22)$$

## NOTE ON SYMMETRY AND DEGENERACY

In most cases we studied, lrLOSC provides a nearly constant energy shift to each isolated group of bands. Core states may be shifted more than valence ones, and the direction of the energy shift depends on the band’s occupancy, but the overall shape of the DFA band structure, as well as the valence and low-lying conduction states’ degeneracies, are generally preserved. The one exception we have observed for this is NaF; in this system, lrLOSC opens a small gap among the four shallow core states (FIG. 1).

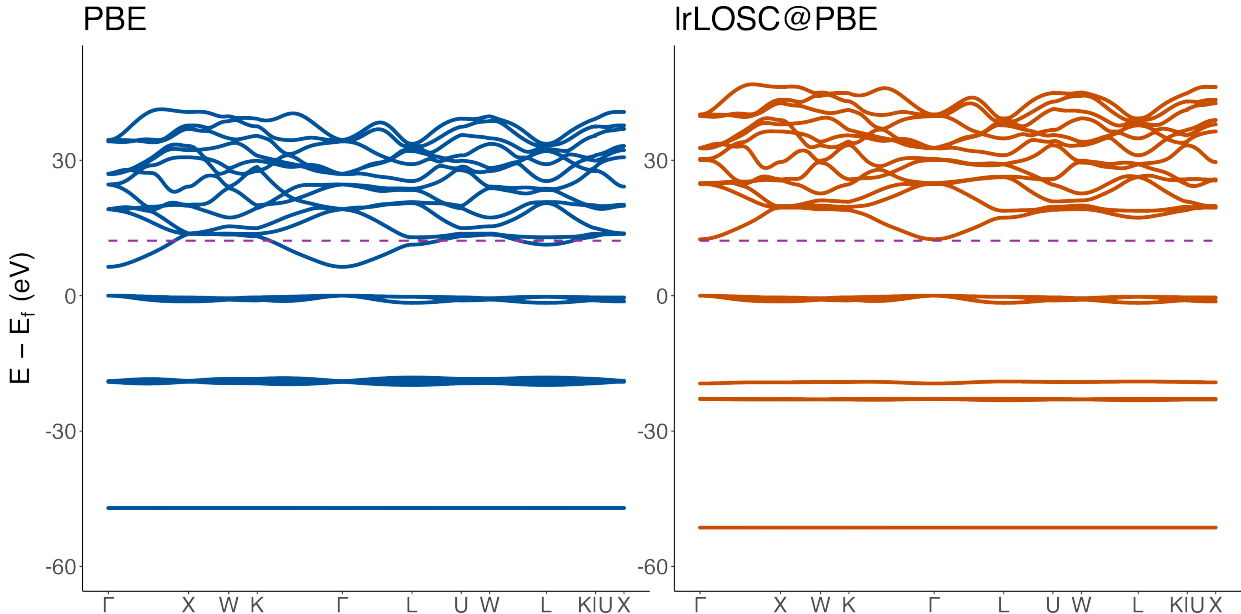


FIG. 1. NaF band structure. Purple dashed line: ZPR-corrected experimental gap.

## VERIFICATION OF THE UNIT CELL-PERIODIC IMPLEMENTATION

The previous implementation of LOSC for materials [9] did not include the monochromatic decomposition; its curvature elements  $\kappa_{\mathbf{R}ij}$  were computed on the large supercell.

We compared the self-Hartree energy

$$J_{ii0}^{\sigma} = \iint d\mathbf{r} d\mathbf{r}' \rho_{0i\sigma}(\mathbf{r})K(|\mathbf{r} - \mathbf{r}'|)\rho_{0i\sigma}(\mathbf{r}') \quad (23)$$

of the DLWFs corresponding to the HOMO and LUMO of water and silicon across the implementations.  $K(r)$  is the Hartree kernel, which can be a bare Coulomb interaction

$K(r) = 1/r$  or (for sLOSC) the attenuated  $K(r) = \text{erfc}(\alpha r)/r$ . The Coulombic divergence in reciprocal space is handled with various corrections: the spherical cutoff (sphcut) [10], Gygi–Baldereschi (G–B) [11] for  $\mathbf{k}$ -sampled systems like Si), or Martyna–Tuckerman (M–T) [12] for isolated systems like water. All computations use the PBE functional [13], and the  $J_{ii0}$  values are in rydbergs.

We simulated a single water molecule in a 25 Å cubic cell, with a kinetic energy cutoff of 100 Ry; to emulate an isolated system, it is sampled only at the origin  $\Gamma$  of the Brillouin zone. We compare it against the in-house QM<sup>4</sup>D code, using the aug-cc-pvTZ basis set. In the tables below, QE–SC refers to the original, supercell-periodic implementation of LOSC, and QE–UC refers to the monochromatically decomposed implementation.

Code	Kernel	Correction	$J_{\text{HOMO}}$	$J_{\text{LUMO}}$
QM <sup>4</sup> D	bare	n/a	1.436	0.413
QE–SC	bare	sphcut	1.442	0.415
QE–UC	bare	M–T	1.442	0.415
QE–UC	bare	sphcut	1.442	0.415
QM <sup>4</sup> D	erfc	n/a	1.110	0.155
QE–SC	erfc	sphcut	1.115	0.157
QE–UC	erfc	none	1.115	0.157

TABLE I. Self-Hartree energy for the DLWFs corresponding to the HOMO and LUMO of water.

We additionally simulated silicon, with the same unit cell as in Table III below; here, however, we used a  $4 \times 4 \times 4$  Monkhorst–Pack mesh centered at  $\Gamma$ , with a 100 Ry kinetic energy cutoff.

The plane-wave codes QE–SC and QE–UC show good agreement with the Gaussian-type orbital code; both the Martyna–Tuckerman and spherical cutoff correction in the monochromatic implementation agree precisely with the spherical cutoff in the supercell-periodic implementation. In Table II, we can see that the spherical cutoff is perfectly replicated in the monochromatic decomposition compared to the supercell-periodic one; however, the Gygi–Baldereschi correction yields a different (and larger) Coulomb repulsion than does the spherical cutoff. The methods are not equivalent; this indicates that a larger  $\mathbf{k}$ -mesh is required to use the spherical cutoff, since with only a  $4 \times 4 \times 4$  mesh some of the Coulomb

Code	Kernel	Divergence	$J_{\text{VBM}}$	$J_{\text{CBM}}$
QE-SC	bare	sphcut	0.525	0.473
QE-UC	bare	G-B	0.555	0.510
QE-UC	bare	sphcut	0.525	0.473
QE-SC	erfc	sphcut	0.258	0.213
QE-UC	erfc	none	0.258	0.213

TABLE II. Self-Hartree energy (Ry) for DLWFs corresponding to the valence band maximum (VBM) and conduction band minimum (CBM) of silicon.

tail is being removed.

Note additionally that the QE-SC implementation can use a the spherical cutoff in addition to the erfc-attenuated kernel; QE-UC cannot combine the two, but the exponential decay is fast enough that the results are numerically equal in the systems tested.

## DATA TABLE

Table III below contains structural parameters, total energy, and band gaps from PBE, lrLOSC, and (where applicable) experiment. The lattice constants  $a$  were taken from Heyd *et al.* [14] and the references therein whenever available, and from Wyckoff [15] otherwise. Experimental band gaps are from Tran and Blaha [16] (LiF, LiCl, Ne, Ar); Poole *et al.* [17] (NaF); and Heyd *et al.* [14] and containing references (C, Si, SiC, Ge, MgO, Bn, BP, AlP). Zero-point renormalization values are computed by Engel *et al.* [18], (C, Si, SiC, LiF, MgO, BN, AlP), Shang *et al.* [19] (BP, LiCl, NaF), and Miglio *et al.* [20] (Ge).

We exclude Ne and Ar from Figure 1 in the main text and from the calculation of the band gap MAE because they do not yet have ZPR calculations available. Observe that lrLOSC underestimates their experimental band gaps, although the result is still much better than PBE's.

---

\* weitao.yang@duke.edu

† Department of Physics, Duke University, Durham, NC 27708, USA

TABLE III. Detailed structural information, total energies, and band gaps. See the Supplemental Material for information on experimental parameters. ZPR is calculated theoretically [18–20]. Error: lrLOSC – electronic gap.

System parameters		Total energy (Ry)		Band gaps (eV)						
Name	Structure	$a$ (Å)	$E_{\text{PBE}}$	$\Delta E_{\text{LOSC}}$	PBE	lrLOSC	Exp.	ZPR	Elec.	Error
C	diamond	3.567	-24.075	$2.10 \times 10^{-5}$	4.205	5.674	5.48	-0.323	5.803	-0.13
Si	diamond	5.43	-16.923	$1.19 \times 10^{-3}$	0.705	1.711	1.17	-0.058	1.228	0.48
SiC	zinblend	4.358	-20.539	$1.72 \times 10^{-4}$	1.356	2.635	2.42	-0.175	2.595	0.04
Ge	diamond	5.658	-357.28	$1.87 \times 10^{-3}$	0.032	0.798	0.74	-0.033	0.773	0.02
MgO	rocksalt	4.207	-152.10	$5.94 \times 10^{-5}$	4.803	8.727	7.22	-0.533	7.753	0.97
LiF	rocksalt	4.017	-63.982	$1.89 \times 10^{-5}$	9.187	15.24	14.20	-1.231	15.431	-0.19
LiCl	rocksalt	5.13	-47.474	$1.34 \times 10^{-4}$	6.329	9.783	9.40	-0.436	9.836	-0.05
NaF	rocksalt	4.62	-140.97	$4.59 \times 10^{-5}$	6.39	12.502	11.50	-0.699	12.199	0.30
BN	zinblend	3.616	-26.805	$1.88 \times 10^{-5}$	4.531	6.387	6.22	-0.402	6.622	-0.23
BP	zinblend	4.538	-19.792	$2.60 \times 10^{-4}$	1.345	2.769	2.40	-0.101	2.501	0.27
AlP	zinblend	5.463	-18.576	$8.40 \times 10^{-4}$	1.576	3.026	2.51	-0.096	2.606	0.42
Ne	cubic	4.429	-66.715	$6.21 \times 10^{-6}$	11.616	19.392	21.70	—	—	—
Ar	cubic	5.256	-45.18	$3.96 \times 10^{-5}$	8.703	14.028	14.20	—	—	—
MAE (eV)									0.28	

- [1] W. Yang, A. J. Cohen, and P. Mori-Sánchez, *J. Chem. Phys.* **136**, 204111 (2012).
- [2] Y. Mei, Z. Chen, and W. Yang, *J. Phys. Chem. Lett.* **12**, 7236 (2021).
- [3] H. J. Monkhorst and J. D. Pack, *Phys. Rev. B* **13**, 5188 (1976).
- [4] S. Baroni, S. de Gironcoli, A. Dal Corso, and P. Giannozzi, *Rev. Mod. Phys.* **73**, 515 (2001).
- [5] I. Timrov, N. Marzari, and M. Cococcioni, *Phys. Rev. B* **98**, 085127 (2018).
- [6] N. Colonna, R. De Gennaro, E. Linscott, and N. Marzari, *J. Chem. Theory Comput.* **18**, 5435 (2022).
- [7] C. Li, X. Zheng, N. Q. Su, and W. Yang, *Nat. Sci. Rev.* **5**, 203 (2018).
- [8] N. Q. Su, A. Mahler, and W. Yang, *J. Phys. Chem. Lett.* **11**, 1528 (2020).
- [9] A. Mahler, J. Williams, N. Q. Su, and W. Yang, *Phys. Rev. B* **106**, 035147 (2022).



- [10] C. A. Rozzi, D. Varsano, A. Marini, E. K. U. Gross, and A. Rubio, *Phys. Rev. B* **73**, 205119 (2006).
- [11] F. Gygi and A. Baldereschi, *Phys. Rev. B* **34**, 4405 (1986).
- [12] G. J. Martyna and M. E. Tuckerman, *The Journal of Chemical Physics* **110**, 2810 (1999).
- [13] J. P. Perdew, K. Burke, and M. Ernzerhof, *Phys. Rev. Lett.* **77**, 3865 (1996).
- [14] J. Heyd, J. E. Peralta, G. E. Scuseria, and R. L. Martin, *J. Chem. Phys.* **123**, 174101 (2005).
- [15] Ralph. W. G. Wyckoff, *Crystal Structures*, 2nd ed. (Wiley, New York, 1973).
- [16] F. Tran and P. Blaha, *Phys. Rev. Lett.* **102**, 226401 (2009).
- [17] R. T. Poole, J. G. Jenkin, J. Liesegang, and R. C. G. Leckey, *Phys. Rev. B* **11**, 5179 (1975).
- [18] M. Engel, H. Miranda, L. Chaput, A. Togo, C. Verdi, M. Marsman, and G. Kresse, *Phys. Rev. B* **106**, 094316 (2022).
- [19] H. Shang, J. Zhao, and J. Yang, *J. Phys. Chem. C* **125**, 6479 (2021).
- [20] A. Miglio, V. Brousseau-Couture, E. Godbout, G. Antonius, Y.-H. Chan, S. G. Louie, M. Côté, M. Giantomassi, and X. Gonze, *npj Comput Mater* **6**, 1 (2020).